

Minor Constraint Disturbances for Deep Semi-supervised Learning

Jielei Chu, *member, IEEE*, Jing Liu, Hongjun Wang,
Zhiguo Gong, *Senior member, IEEE*, Tianrui Li, *Senior member, IEEE*



arXiv:2003.06321v1 [cs.LG] 13 Mar 2020

Abstract—In high-dimensional data space, semi-supervised feature learning based on Euclidean distance shows instability under a broad set of conditions. Furthermore, the scarcity and high cost of labels prompt us to explore new semi-supervised learning methods with the fewest labels. In this paper, we develop a novel Minor Constraint Disturbances-based Deep Semi-supervised Feature Learning framework (MCD-DSFL) from the perspective of probability distribution for feature representation. There are two fundamental modules in the proposed framework: one is a Minor Constraint Disturbances-based restricted Boltzmann machine with Gaussian visible units (MCDGRBM) for modelling continuous data and the other is a Minor Constraint Disturbances-based restricted Boltzmann machine (MCDRBM) for modelling binary data. The Minor Constraint Disturbances (MCD) consist of less instance-level constraints which are produced by only two randomly selected labels from each class. The Kullback-Leibler (KL) divergences of the MCD are fused into the Contrastive Divergence (CD) learning for training the proposed MCDGRBM and MCDRBM models. Then, the probability distributions of hidden layer features are as similar as possible in the same class and they are as dissimilar as possible in the different classes simultaneously. Despite the weak influence of the MCD for our shallow models (MCDGRBM and MCDRBM), the proposed deep MCD-DSFL framework improves the representation capability significantly under its leverage effect. The semi-supervised strategy based on the KL divergence of the MCD significantly reduces the reliance on the labels and improves the stability of the semi-supervised feature learning in high-dimensional space simultaneously. Experimental results demonstrate that the proposed framework shows more excellent performance than state-of-the-art semi-supervised shallow models and deep feature learning methods for clustering.

Index Terms—Minor constraint disturbances; deep semi-supervised learning; restricted Boltzmann machine; semi-supervised clustering.

1 INTRODUCTION

Semi-supervised learning methodology has long been one of focus on feature learning because of the scarcity and high cost of labels. There are various semi-supervised learning methods which are

Jielei Chu, Hongjun Wang, Tianrui Li (the corresponding author) are with the Institute of Artificial Intelligence, School of Information Science and Technology, Southwest Jiaotong University, Chengdu 611756, China. Tianrui Li is also with National Engineering Laboratory of Integrated Transportation Big Data Application Technology, Southwest Jiaotong University, Chengdu 611756, China. e-mails: {jieleichu, wanghongjun, trli}@swjtu.edu.cn.

Jing Liu is with the School of Business, Sichuan University, Sichuan, 610065, Chengdu, China. e-mail: liujing@scu.edu.cn

Zhiguo Gong is with the State Key Laboratory of Internet of Things for Smart City, Department of Computer and Information Science, University of Macau, Macau, China. Email: fstzgg@um.edu.mo

widely used in classification [1], [2], [3], [4], clustering [5], [6], semantic segmentation [7], discrete choice models [8], sentiment analysis [9], facial expression recognition [10], fault diagnosis [11], face beauty prediction [12], brain tissue segmentation [13] and so on. In these applications, semi-supervised feature learning [14], [15] is a critical phase to enhance the efficiencies and performances of the following learning tasks. The current semi-supervised feature learning method is divided into shallow mode and deep learning frameworks.

Existing shallow semi-supervised feature learning methods [16], [17], [18], [19] exploit various semi-supervised strategies to improve learning efficiency and performance while minimize the use of labels. To tackle both the heterogeneous and homogeneous problems, Li and Zhang [16] proposed a semi-supervised covariance matching approach used a few labelled samples. The Non-negative Matrix Factorization (NMF) is a well-known dimensionality reduction method. Jia et al. [17] developed a semi-supervised NMF model which takes advantage of the labels to guide the factorization. In order to modeling the label information in semi-supervised NMF, the work uses a similarity regularization term to encourage the low-dimensional representations with different labels to be dissimilar. Moreover it uses a dissimilarity regularization term to restrict the similarity among data samples with the same labels and few unlabeled samples in the low dimensional representations space. Chen et al. [18] presented a Sparse Rescaled Linear Square Regression (SRLSR) method which has capability to obtain more sparse regression coefficients for semi-supervised feature learning. In our previous work [19], we developed a shallow semi-supervised feature learning neural network model called pairwise constraints restricted Boltzmann machine with Gaussian visible units (pcGRBM) which uses *Must-link* and *Cannot-link* information of reconstructed data samples to guide the procedure of feature learning. The pcGRBM model uses European distance of *Must-link* and *Cannot-link* information to optimize critical connection parameters. This semi-supervised strategy enhances the representation capability of the hidden layer, but the following learning tasks show inevitable instability with the hidden features of the pcGRBM. As we all know, Euclidean distance function has instability in high-dimensional space [19], [20]. So, we present a novel deep semi-supervised strategy from the perspective of probability distributions of Minor Constraint Disturbances (MCD) to improve feature distribution of hidden layers in this paper.

In most cases, deep feature learning [21], [22], [23], [24] shows outstanding representation capability. Thus, there are some

works recently explore deep semi-supervised learning method [25], [26] which not only retains or even promotes the capabilities of deep feature learning but also reduces the reliance on labels as few as possible. In general, the conventional semi-supervised learning methods perform within a fixed feature space. The DCS [27] is an incremental deep semi-supervised learning method, which propagates information from labeled to unlabeled samples in the procedure of deep feature learning. In the DCS framework, the Co-Space stems from two CNN models by extracting features for all unlabeled and labeled samples. Sellami et al. [28] constructed a semi-supervised 3-D Convolutional Neural Network (3-D CNN) for the spectro-spatial classification. The approach not only preserves the information of the relevant spectro-spatial but also enhances the classification using few labeled samples. Xue et al. [29] proposed an efficient and fast semi-supervised DIOD method based on weakly deep semi-supervised joint sparse learning and Advanced Region Proposal Networks (ARPNs). To solve the mobile traffic Anomaly Detection (AD) problem, Trinh et al. [30] developed a comprehensive deep semi-supervised framework based on Long Short-Term Memory (LSTM). In computer vision, the object detection of inverse synthetic aperture radar is a challenging problem. This semi-supervised method only needs one class of samples. Meng et al. [31] presented a Semi-supervised Graph Regularized Deep NMF (SGDNMF) with bi-orthogonal constraints for data representation. The bi-orthogonal constraints are introduced into the SGDNMF model on two factor matrices for improving the representation performance with a small fraction of labels. The intelligent diagnostic system has been an increasing interest in the industrial applications. Kurup et al. [10] illustrated a semi-supervised feature selection method for facial expression recognition with a Deep Belief Network (DBN). The semi-supervised DBN improves the classification accuracy using the available labeled data and unlabelled observations. Razavi-Far et al. [11] developed a Semi-Supervised Deep Ladder Network for diagnosing gear faults. The deep semi-supervised-learning scheme consists of an information fusion module and a decision making module. The deep semi-supervised learning procedure is used in the decision making module to maximize the diagnostic efficiency and simultaneously minimize the human interaction. To reduce the inputs for modelling in the learning process, Aboozar et al. [15] designed a Deep Feature Selection (Deep-FS) algorithm based on Deep Boltzmann Machine (DBM). The Deep-FS model embeds feature selection in a restricted boltzmann machine (RBM) [32], [33] which is used for training a DBM and can remove some irrelevant features which negatively impact on feature representation. Mercado et al. [34] proposed a semi-supervised learning method on Multilayer Graphs (semi-MG) using a regularizer of the generalized matrix mean. In each individual graph layer, the labeled and unlabeled samples are fused together with the encoding information. The works of [15] and [34] are the most closely related work with our framework for deep semi-supervised learning.

In this paper, we propose a novel deep semi-supervised feature learning framework from the perspective of probability distribution of the MCD in hidden layers. The Kullback-Leibler (KL) divergences [35], [36], [37] of the MCD are fused into the Contrastive Divergence (CD) learning in the training process. Our main contributions are summarized as follows:

- A Minor Constraint Disturbances-based GRBM (MCD-GRBM) for modelling continuous data and a Minor Con-

straint Disturbances-based RBM (MCDRBM) for modelling binary data are proposed from the perspective of probability distribution instead of Euclidean distance of the MCD. The KL divergences of the MCD are fused into CD learning for training the proposed MCDGRBM and MCDRBM models. The semi-supervised strategy based on the KL divergence of the MCD significantly reduces the reliance on the labels and improves the stability of the semi-supervised feature learning in high-dimensional space simultaneously.

- A novel Minor Constraint Disturbances-based Deep Semi-supervised Feature Learning framework (MCD-DSFL) is developed for deep semi-supervised feature representation. Despite the weak influence of the MCD for our shallow models (MCDGRBM and MCDRBM), the proposed MCD-DSFL framework improves the deep representation capability significantly under its the leverage effect.
- The experimental results demonstrate that the MCD-DSFL framework shows more excellent performance than state-of-the-art semi-supervised shallow models and deep feature learning frameworks. Furthermore, the scale coefficient shows positive effectiveness for the feature learning of our framework.

The rest of the paper is organized as follows. Section 2 introduces the theoretical background. Section 3 presents two new shallow MCDGRBM and MCDRBM models. Section 4 illustrates a novel deep semi-supervised feature learning framework, MCD-DSFL. Section 5 shows all experimental results. Finally, Section 6 summarizes our contributions.

2 BACKGROUND

2.1 Kullback-Leibler Divergence

The KL divergence [35], [36], [37] is a popular measure of the similarity (closeness) between two discrete distributions P and Q , defined by

$$\mathbf{KL}(P \parallel Q) = \sum_x P(x) \log \frac{P(x)}{Q(x)} \quad (1)$$

where KL divergence is always non-negative ($\mathbf{KL}(P \parallel Q) \geq 0$) and $\mathbf{KL}(P \parallel Q) = 0$ if and only if $P = Q$. In other words, KL divergence is the expectation of the logarithmic difference between P and Q . To obtain a distribution P which is the closest to Q , we can minimize KL divergence of them.

In neural networks, the method of updating parameters often directs towards minimizing the KL divergence [38]. KL divergence is used to measure the similarity between uncertain objects, then it can be merged with learning algorithms to improve the performance [39]. In computer vision, the KL divergence is used in training rotation-invariant RBM [40] which can offer stability and consistency of representation. In variational Bayes Recurrent Neural Networks (BRNNs) [41], the KL divergence between the approximate posterior and the prior distributions is a vital component of the models.

2.2 Contrastive Divergence Learning

CD learning [42], [43] as a fast learning method has been successfully applied to train RBMs. It proximately follows the gradient of two KL divergences and is defined as

$$\mathbf{CD}_n = \mathbf{KL}(p_0 \parallel p_\infty) - \mathbf{KL}(p_n \parallel p_\infty), \quad (2)$$

where p_0 is the data distribution, p_∞ is model distribution and p_n is the distribution of the data after running the Markov chain for n step.

In the encoding process of RBMs model, the conditional probability $p(h_j = 1|\mathbf{v})$ is given by:

$$p(h_j = 1|\mathbf{v}) = \sigma(b_j + \sum_i v_i w_{ij}), \quad (3)$$

where $\mathbf{v} = (v_1, v_2, \dots, v_i, \dots, v_n)$ is a vector of visible layer, σ is the sigmoid function, w_{ij} is the connection parameter between the hidden and visible layers, b_j is bias parameter of hidden layers. In the reconstructed process of RBMs, the conditional probability $p(v_i = 1|\mathbf{h})$ is given by:

$$p(v_i = 1|\mathbf{h}) = \sigma(c_i + \sum_j h_j w_{ij}), \quad (4)$$

where $\mathbf{h} = (h_1, h_2, \dots, h_j, \dots, h_m)$ is a vector of hidden layer, c_i is bias parameter of visible layer.

In the GRBM and its variants [19], [44], [45], the hidden layers remain unchanged binary units, but visible layer units are replaced by Gaussian linear units. The conditional probability of reconstructed process takes the form

$$p(\mathbf{v}|\mathbf{h}) = \mathcal{N}(\sum \mathbf{h} \mathbf{W}^T + \mathbf{c}, \sigma^2), \quad (5)$$

where $\mathbf{c} = (c_1, c_2, \dots, c_i, \dots, c_n)$, $\mathbf{W}_{n \times m}$ is a connection matrix, $\mathcal{N}(\cdot)$ is a gaussian density.

For fast training RBMs, CD learning with one step Gibbs sampling (CD-1 learning) [43] is defined by:

$$\mathbf{CD}_1 = \mathbf{KL}(p_0||p_\infty) - \mathbf{KL}(p_1||p_\infty), \quad (6)$$

where p_1 is the distribution of the reconstructed data. Then the update rules of model parameters of RBMs are given by

$$w_{ij}^{(\tau+1)} = w_{ij}^{(\tau)} + \varepsilon(\langle v_i h_j \rangle_0 - \langle v_i h_j \rangle_1) \quad (7)$$

$$b_j^{(\tau+1)} = b_j^{(\tau)} + \varepsilon(\langle h_j \rangle_0 - \langle h_j \rangle_1) \quad (8)$$

and

$$c_i^{(\tau+1)} = c_i^{(\tau)} + \varepsilon(\langle v_i \rangle_0 - \langle v_i \rangle_1) \quad (9)$$

where $\langle \cdot \rangle_0$ denotes an average concerning the data distribution, $\langle \cdot \rangle_1$ denotes an average concerning the reconstructed data distribution and ε is learning rate.

3 THE MCDRBM AND MCDGRBM MODELS

This section introduces the MCDRBM for modelling binary data and the MCDGRBM model for modelling continuous data. They are the fundamental modules in our MCD-DSFL deep framework.

3.1 Problem Definition

The main goal here is to develop novel variants of RBM and GRBM models to enhance their representation capabilities with the MCD in hidden layers from the perspective of probability distribution instead of Euclidean distance.

Firstly, we randomly select two labels from each class to generate the two-tuples set of the MCD for modelling the MCDRBM model. Let a dataset has K clusters, then the MCD set contains two subsets. One is within-cluster constraints (\mathcal{WCC}) subset which

has K instance-level constraints and the elements of each two-tuple of \mathcal{WCC} subset come from the same cluster. And the other is between-cluster constraints (\mathcal{BCC}) subset and the elements of each two-tuple of \mathcal{BCC} subset come from different clusters. The KL divergences of the MCD in \mathcal{WCC} and \mathcal{BCC} sets are fused into CD learning in the process of encoding of the MCDRBM models.

Given a visible layer data set of the MCDRBM model $\mathcal{V} = \{\mathbf{v}_1, \mathbf{v}_2, \dots, \mathbf{v}_i, \dots, \mathbf{v}_M\}$, where $\mathbf{v}_i = (v_{i1}, v_{i2}, \dots, v_{ij}, \dots, v_{in})$, M is the number of instance vector and n is the dimensionality of the visible layer. Each visible layer instance corresponds to a feature vector in the hidden layer. Denote the hidden feature vector sets of the MCDRBM model as $\mathcal{H} = \{\mathbf{h}_1, \mathbf{h}_2, \dots, \mathbf{h}_i, \dots, \mathbf{h}_M\}$, where m is the dimensionality of hidden layer and \mathbf{h}_i is the hidden feature of \mathbf{v}_i . Similarly, we denote the visible layer data of the MCDGRBM model and its corresponding hidden feature set as $\tilde{\mathcal{V}} = \{\tilde{\mathbf{v}}_1, \tilde{\mathbf{v}}_2, \dots, \tilde{\mathbf{v}}_i, \dots, \tilde{\mathbf{v}}_M\}$ and $\tilde{\mathcal{H}} = \{\tilde{\mathbf{h}}_1, \tilde{\mathbf{h}}_2, \dots, \tilde{\mathbf{h}}_i, \dots, \tilde{\mathbf{h}}_M\}$, respectively. We expect the probability distribution between the elements of two-tuples in \mathcal{WCC} subset to be as similar as possible in the encoding process. Moreover, we also expect the probability distribution between the elements of two-tuples in \mathcal{BCC} subset to be as dissimilar as possible in encoding process. Combining two minor constraints, the optimisation problem of the MCD for the MCDRBM model is given by:

$$\min \left\{ \frac{1}{K_w} \sum_{\mathcal{WCC}} \mathbf{KL}(P(\mathbf{h}_f|\mathbf{v}_f) \| P(\mathbf{h}_g|\mathbf{v}_g)) - \frac{1}{K_b} \sum_{\mathcal{BCC}} \mathbf{KL}(P(\mathbf{h}_r|\mathbf{v}_r) \| P(\mathbf{h}_s|\mathbf{v}_s)) \right\}, \quad (10)$$

where $(\mathbf{v}_f, \mathbf{v}_g) \in \mathcal{WCC}$ and $(\mathbf{v}_r, \mathbf{v}_s) \in \mathcal{BCC}$, K_w and K_b are the numbers of the instance-level constraints of \mathcal{WCC} and \mathcal{BCC} , respectively. Similarly, the optimisation problem of the MCD for the MCDGRBM model is given by:

$$\min \left\{ \frac{1}{\widetilde{K}_w} \sum_{\widetilde{\mathcal{WCC}}} \mathbf{KL}(P(\tilde{\mathbf{h}}_f|\tilde{\mathbf{v}}_f) \| P(\tilde{\mathbf{h}}_g|\tilde{\mathbf{v}}_g)) - \frac{1}{\widetilde{K}_b} \sum_{\widetilde{\mathcal{BCC}}} \mathbf{KL}(P(\tilde{\mathbf{h}}_r|\tilde{\mathbf{v}}_r) \| P(\tilde{\mathbf{h}}_s|\tilde{\mathbf{v}}_s)) \right\}, \quad (11)$$

where $(\tilde{\mathbf{v}}_f, \tilde{\mathbf{v}}_g) \in \widetilde{\mathcal{WCC}}$ and $(\tilde{\mathbf{v}}_r, \tilde{\mathbf{v}}_s) \in \widetilde{\mathcal{BCC}}$, $\widetilde{\mathcal{WCC}}$ and $\widetilde{\mathcal{BCC}}$ are the within-cluster and between-cluster constraints subsets which have \widetilde{K}_w and \widetilde{K}_b two-tuples, respectively.

3.2 The Model

In this subsection, we present the MCDRBM and MCDGRBM models: novel variant of RBM and GRBM designed to improve representation capability by fusing the KL divergence of the MCD into the CD learning [42], [43]. We expect that the probability distributions of hidden layer features are as similar as possible in the same class under the effect of the MCD. Simultaneously, we also expect that they are as dissimilar as possible in different classes. Thus, the objective function of the MCDRBM model can be defined to be:

$$\begin{aligned} \mathcal{L}(\mathcal{V}) = & -(1 - \gamma) \left(\mathbf{KL}(p_0 \| p_\infty) - \mathbf{KL}(p_1 \| p_\infty) \right) \\ & + \gamma \left[\frac{1}{K_w} \sum_{\mathcal{WCC}} \mathbf{KL}(P(\mathbf{h}_f|\mathbf{v}_f) \| P(\mathbf{h}_g|\mathbf{v}_g)) \right. \\ & \left. - \frac{1}{K_b} \sum_{\mathcal{BCC}} \mathbf{KL}(P(\mathbf{h}_r|\mathbf{v}_r) \| P(\mathbf{h}_s|\mathbf{v}_s)) \right], \quad (12) \end{aligned}$$

where $\gamma \in (0, 1)$ is a scale coefficient. Similarly, the objective function of the MCDGRBM model can be defined to be:

$$\begin{aligned} \mathcal{G}(\tilde{\mathbf{V}}) = & -(1 - \gamma) \left(\mathbf{KL}(\tilde{p}_0 \parallel \tilde{p}_\infty) - \mathbf{KL}(\tilde{p}_1 \parallel \tilde{p}_\infty) \right) \\ & + \gamma \left[\frac{1}{\tilde{K}_w} \sum_{\tilde{WCC}} \mathbf{KL}(P(\tilde{\mathbf{h}}_f | \tilde{\mathbf{v}}_f) \parallel P(\tilde{\mathbf{h}}_g | \tilde{\mathbf{v}}_g)) \right. \\ & \left. - \frac{1}{\tilde{K}_b} \sum_{\tilde{BCC}} \mathbf{KL}(P(\tilde{\mathbf{h}}_r | \tilde{\mathbf{v}}_r) \parallel P(\tilde{\mathbf{h}}_s | \tilde{\mathbf{v}}_s)) \right], \end{aligned} \quad (13)$$

Next, we give a detailed inference of the MCDGRBM model. Since the approximate gradient of $\mathbf{KL}(p_0 \parallel p_\infty) - \mathbf{KL}(p_1 \parallel p_\infty)$ is particularly easy to calculate:

$$-\frac{\partial}{\partial w_{ij}} (\mathbf{KL}(p_0 \parallel p_\infty) - \mathbf{KL}(p_1 \parallel p_\infty)) \approx \langle v_i h_j \rangle_0 - \langle v_i h_j \rangle_1, \quad (14)$$

$$-\frac{\partial}{\partial b_j} (\mathbf{KL}(p_0 \parallel p_\infty) - \mathbf{KL}(p_1 \parallel p_\infty)) \approx \langle h_j \rangle_0 - \langle h_j \rangle_1 \quad (15)$$

and

$$-\frac{\partial}{\partial c_i} (\mathbf{KL}(p_0 \parallel p_\infty) - \mathbf{KL}(p_1 \parallel p_\infty)) \approx \langle v_i \rangle_0 - \langle v_i \rangle_1. \quad (16)$$

To obtain the update rules of model parameters, the main task is to solve the gradient of $\frac{1}{\tilde{K}_w} \sum_{\tilde{WCC}} \mathbf{KL}(P(\tilde{\mathbf{h}}_f | \tilde{\mathbf{v}}_f) \parallel P(\tilde{\mathbf{h}}_g | \tilde{\mathbf{v}}_g)) - \frac{1}{\tilde{K}_b} \sum_{\tilde{BCC}} \mathbf{KL}(P(\tilde{\mathbf{h}}_r | \tilde{\mathbf{v}}_r) \parallel P(\tilde{\mathbf{h}}_s | \tilde{\mathbf{v}}_s))$.

3.3 The Update Rules of Model Parameters

Firstly, we compute the gradient of $\mathbf{KL}(P(\mathbf{h}_f | \mathbf{v}_f) \parallel P(\mathbf{h}_g | \mathbf{v}_g))$. Before calculating the gradient, an equivalent transformation of it takes the form:

$$\begin{aligned} & \mathbf{KL}(P(\mathbf{h}_f | \mathbf{v}_f) \parallel P(\mathbf{h}_g | \mathbf{v}_g)) \\ & = \sum_x p(h_{fx} = 1 | \mathbf{v}_f) \log \frac{p(h_{fx} = 1 | \mathbf{v}_f)}{p(h_{gx} = 1 | \mathbf{v}_g)} \\ & = \sum_x \left[p(h_{fx} = 1 | \mathbf{v}_f) \log p(h_{fx} = 1 | \mathbf{v}_f) \right. \\ & \quad \left. - p(h_{fx} = 1 | \mathbf{v}_f) \log p(h_{gx} = 1 | \mathbf{v}_g) \right]. \end{aligned} \quad (17)$$

Then, the gradient $\frac{\partial}{\partial w_{ij}} \mathbf{KL}(P(\mathbf{h}_f | \mathbf{v}_f) \parallel P(\mathbf{h}_g | \mathbf{v}_g))$ is given by:

$$\begin{aligned} & \frac{\partial}{\partial w_{ij}} \mathbf{KL}(P(\mathbf{h}_f | \mathbf{v}_f) \parallel P(\mathbf{h}_g | \mathbf{v}_g)) = \\ & \sum_x \left[\frac{\partial}{\partial w_{ij}} p(h_{fx} = 1 | \mathbf{v}_f) \log p(h_{fx} = 1 | \mathbf{v}_f) + \right. \\ & \quad \left. \frac{\partial}{\partial w_{ij}} p(h_{fx} = 1 | \mathbf{v}_f) - \frac{\partial}{\partial w_{ij}} p(h_{fx} = 1 | \mathbf{v}_f) \log p(h_{gx} = 1 | \mathbf{v}_g) \right. \\ & \quad \left. - \frac{p(h_{fx} = 1 | \mathbf{v}_f) \frac{\partial}{\partial w_{ij}} p(h_{gx} = 1 | \mathbf{v}_g)}{p(h_{gx} = 1 | \mathbf{v}_g)} \right] \\ & = \sum_x \left\{ \frac{\partial}{\partial w_{ij}} p(h_{fx} = 1 | \mathbf{v}_f) \left[\log p(h_{fx} = 1 | \mathbf{v}_f) \right. \right. \\ & \quad \left. \left. + \log p(h_{gx} = 1 | \mathbf{v}_g) + 1 \right] - \frac{p(h_{fx} = 1 | \mathbf{v}_f) \frac{\partial}{\partial w_{ij}} p(h_{gx} = 1 | \mathbf{v}_g)}{p(h_{gx} = 1 | \mathbf{v}_g)} \right\}. \end{aligned} \quad (18)$$

In encoding procedure, the transformation from the visible layer to the hidden layer is the sigmoid transform. So, the gradient $\frac{\partial}{\partial w_{ij}} p(h_{fx} = 1 | \mathbf{v}_f)$ takes the form:

$$\frac{\partial}{\partial w_{ij}} p(h_{fx} = 1 | \mathbf{v}_f) = \frac{\partial}{\partial w_{ij}} \sigma(b_x + \sum_i v_{fi} w_{ix}). \quad (19)$$

When $x = j$, it is easy to obtain the gradient $\frac{\partial}{\partial w_{ij}} p(h_{fx} = 1 | \mathbf{v}_f)$ as follows.

$$\begin{aligned} \frac{\partial}{\partial w_{ij}} p(h_{fx} = 1 | \mathbf{v}_f) & = \frac{v_{fi} e^{-(b_j + \sum_i v_{fi} w_{ij})}}{(1 + e^{-(b_j + \sum_i v_{fi} w_{ij})})^2} \\ & = h_{fj} (1 - h_{fj}) v_{fi} \end{aligned} \quad (20)$$

In other cases, $\frac{\partial}{\partial w_{ij}} p(h_{fx} = 1 | \mathbf{v}_f) = 0$. Similarly, the gradient $\frac{\partial}{\partial w_{ij}} p(h_{gx} = 1 | \mathbf{v}_g)$ takes the form:

$$\frac{\partial}{\partial w_{ij}} p(h_{gx} = 1 | \mathbf{v}_g) = h_{gj} (1 - h_{gj}) v_{gi}. \quad (21)$$

From Eqs. (18), (20) and (21), we obtain the gradient $\frac{\partial}{\partial w_{ij}} \mathbf{KL}(P(\mathbf{h}_f | \mathbf{v}_f) \parallel P(\mathbf{h}_g | \mathbf{v}_g))$ as follows.

$$\begin{aligned} & \frac{\partial}{\partial w_{ij}} \mathbf{KL}(P(\mathbf{h}_f | \mathbf{v}_f) \parallel P(\mathbf{h}_g | \mathbf{v}_g)) \\ & = v_{fi} h_{fj} (1 - h_{fj}) (\log h_{fj} + \log h_{gj} + 1) - v_{gi} h_{gj} (1 - h_{gj}). \end{aligned} \quad (22)$$

Similarly, the gradient $\frac{\partial}{\partial w_{ij}} \mathbf{KL}(P(\mathbf{h}_r | \mathbf{v}_r) \parallel P(\mathbf{h}_s | \mathbf{v}_s))$ is given by:

$$\begin{aligned} & \frac{\partial}{\partial w_{ij}} \mathbf{KL}(P(\mathbf{h}_r | \mathbf{v}_r) \parallel P(\mathbf{h}_s | \mathbf{v}_s)) \\ & = v_{ri} h_{rj} (1 - h_{rj}) (\log h_{rj} + \log h_{sj} + 1) - v_{si} h_{sj} (1 - h_{sj}). \end{aligned} \quad (23)$$

Therefore, we obtain the update rules of \mathbf{W} from Eqs. (14), (22) and (23) which take the form:

$$\begin{aligned} w_{ij}^{(\tau+1)} & = w_{ij}^{(\tau)} + (1 - \gamma) \varepsilon (\langle v_i h_j \rangle_0 - \langle v_i h_j \rangle_1) + \frac{\gamma}{\tilde{K}_w} \sum_{\tilde{WCC}} \\ & \quad \left[v_{fi} h_{fj} (1 - h_{fj}) (\log h_{fj} + \log h_{gj} + 1) - v_{gi} h_{gj} (1 - h_{gj}) \right] \\ & \quad - \frac{\gamma}{\tilde{K}_b} \sum_{\tilde{BCC}} \left[v_{ri} h_{rj} (1 - h_{rj}) (\log h_{rj} + \log h_{sj} + 1) \right. \\ & \quad \left. - v_{si} h_{sj} (1 - h_{sj}) \right] \end{aligned} \quad (24)$$

where ε is a learning rate. In the following, we infer the update rule of parameter \mathbf{b} .

When $x = j$, it is easy to obtain the gradients $\frac{\partial}{\partial b_j} \mathbf{KL}(P(\mathbf{h}_f | \mathbf{v}_f) \parallel P(\mathbf{h}_g | \mathbf{v}_g))$ and $\frac{\partial}{\partial b_j} \mathbf{KL}(P(\mathbf{h}_r | \mathbf{v}_r) \parallel P(\mathbf{h}_s | \mathbf{v}_s))$ as follows.

$$\begin{aligned} & \frac{\partial}{\partial b_j} \mathbf{KL}(P(\mathbf{h}_f | \mathbf{v}_f) \parallel P(\mathbf{h}_g | \mathbf{v}_g)) \\ & = h_{fj} (1 - h_{fj}) (\log h_{fj} + \log h_{gj} + 1) - h_{gj} (1 - h_{gj}) \end{aligned} \quad (25)$$

and

$$\begin{aligned} & \frac{\partial}{\partial b_j} \mathbf{KL}(P(\mathbf{h}_r | \mathbf{v}_r) \parallel P(\mathbf{h}_s | \mathbf{v}_s)) \\ & = h_{rj} (1 - h_{rj}) (\log h_{rj} + \log h_{sj} + 1) - h_{sj} (1 - h_{sj}). \end{aligned} \quad (26)$$

Then, we obtain the update rule of \mathbf{b} from Eqs. (15), (24) and (26) which takes the form:

$$\begin{aligned} b_j^{(\tau+1)} &= b_j^{(\tau)} + (1 - \gamma)\varepsilon(\langle h_j \rangle_0 - \langle h_j \rangle_1) + \\ &\frac{\gamma}{K_w} \sum_{WCC} [h_{fj}(1 - h_{fj})(\log h_{fj} + \log h_{gj} + 1) - \\ &h_{gj}(1 - h_{gj})] - \frac{\gamma}{K_b} \sum_{BCC} [h_{rj}(1 - h_{rj})(\log h_{rj} + \log h_{sj} \\ &+ 1) - h_{sj}(1 - h_{sj})] \end{aligned} \quad (27)$$

As for model parameter \mathbf{c} , it's obvious that

$$\frac{\partial}{\partial c_i} \mathbf{KL}(P(\mathbf{h}_f | \mathbf{v}_f) \| P(\mathbf{h}_g | \mathbf{v}_g)) = 0 \quad (28)$$

and

$$\frac{\partial}{\partial c_i} \mathbf{KL}(P(\mathbf{h}_r | \mathbf{v}_r) \| P(\mathbf{h}_s | \mathbf{v}_s)) = 0. \quad (29)$$

From Eqs. (16), (28) and (29) the update rule of \mathbf{c} takes the form:

$$c_i^{(\tau+1)} = c_i^{(\tau)} + (1 - \gamma)\varepsilon(\langle v_i \rangle_0 - \langle v_i \rangle_1) \quad (30)$$

Finally, the update rules of \mathbf{W} , \mathbf{b} and \mathbf{c} of the MCDRBM model are Eqs. (24), (27) and (30), respectively.

In the MCDGRBM model, the hidden units remain binary, but the visible units are the linear units with Gaussian noise. Then, in the encoding process of MCDGRBM model, the conditional probability $p(h_j = 1 | \tilde{\mathbf{v}})$ is given by:

$$p(\tilde{h}_j = 1 | \tilde{\mathbf{v}}) = \sigma(\tilde{b}_j + \sum_i \tilde{v}_i \tilde{w}_{ij}) \quad (31)$$

and its conditional probability of reconstructed process takes the form:

$$p(\tilde{\mathbf{v}} | \tilde{\mathbf{h}}) = \mathcal{N}(\sum \tilde{\mathbf{h}} \tilde{\mathbf{W}}^T + \tilde{\mathbf{c}}, \sigma^2). \quad (32)$$

The update rules of the parameters $\tilde{\mathbf{W}}$, $\tilde{\mathbf{b}}$ and $\tilde{\mathbf{c}}$ of the MCDGRBM model are similar to the MCDRBM model, which take the form:

$$\begin{aligned} \tilde{w}_{ij}^{(\tau+1)} &= \tilde{w}_{ij}^{(\tau)} + (1 - \gamma)\varepsilon(\langle \tilde{v}_i \tilde{h}_j \rangle_0 - \langle \tilde{v}_i \tilde{h}_j \rangle_1) + \frac{\gamma}{K_w} \sum_{WCC} \\ &\left[\tilde{v}_{fi} \tilde{h}_{fj} (1 - \tilde{h}_{fj}) (\log \tilde{h}_{fj} + \log \tilde{h}_{gj} + 1) - \tilde{v}_{gi} \tilde{h}_{gj} (1 - \tilde{h}_{gj}) \right] \\ &- \frac{\gamma}{K_b} \sum_{BCC} \left[\tilde{v}_{ri} \tilde{h}_{rj} (1 - \tilde{h}_{rj}) (\log \tilde{h}_{rj} + \log \tilde{h}_{sj} + 1) \right. \\ &\left. - \tilde{v}_{si} \tilde{h}_{sj} (1 - \tilde{h}_{sj}) \right], \end{aligned} \quad (33)$$

$$\begin{aligned} \tilde{b}_j^{(\tau+1)} &= \tilde{b}_j^{(\tau)} + (1 - \gamma)\varepsilon(\langle \tilde{h}_j \rangle_0 - \langle \tilde{h}_j \rangle_1) + \\ &\frac{\gamma}{K_w} \sum_{WCC} [\tilde{h}_{fj}(1 - \tilde{h}_{fj})(\log \tilde{h}_{fj} + \log \tilde{h}_{gj} + 1) - \\ &\tilde{h}_{gj}(1 - \tilde{h}_{gj})] - \frac{\gamma}{K_b} \sum_{BCC} [\tilde{h}_{rj}(1 - \tilde{h}_{rj})(\log \tilde{h}_{rj} + \log \tilde{h}_{sj} \\ &+ 1) - \tilde{h}_{sj}(1 - \tilde{h}_{sj})] \end{aligned} \quad (34)$$

and

$$\tilde{c}_i^{(\tau+1)} = \tilde{c}_i^{(\tau)} + (1 - \gamma)\varepsilon(\langle \tilde{v}_i \rangle_0 - \langle \tilde{v}_i \rangle_1) \quad (35)$$

3.4 Learning Algorithms

In this subsection, we show the learning algorithm of the proposed shallow MCDRBM and MCDGRBM models according to the update rules of its parameters.

Algorithm 1: MCDRBM learning

Input:

$\mathcal{V} = \{\mathbf{v}_1, \mathbf{v}_2, \dots, \mathbf{v}_i, \dots, \mathbf{v}_N\}$: visible layer data;
MCD: a set of minor constraint disturbances.

Output:

\mathbf{W} , \mathbf{b} and \mathbf{c} : the parameters of MCDRBM.

Step 1: Randomly initialize \mathbf{W} , \mathbf{b} and \mathbf{c} .

Step 2: Sample the states of the hidden layer units by Eq. (3).

Step 3: Sample the states of the reconstructed visible layer units by Eq. (4).

Step 4: Update \mathbf{W} parameter by Eq. (24).

Step 5: Update \mathbf{b} parameter by Eq. (27).

Step 6: Update \mathbf{c} parameter by Eq. (30).

Step 7: **While** iteration less than maximum **go to** Step 2.

step 8: **return** \mathbf{W} , \mathbf{b} and \mathbf{c} .

Algorithm 2: MCDGRBM learning

Input:

$\tilde{\mathcal{V}} = \{\tilde{\mathbf{v}}_1, \tilde{\mathbf{v}}_2, \dots, \tilde{\mathbf{v}}_i, \dots, \tilde{\mathbf{v}}_N\}$: visible layer data;
MCD: a set of minor constraint disturbances.

Output:

$\tilde{\mathbf{W}}$, $\tilde{\mathbf{b}}$ and $\tilde{\mathbf{c}}$: the parameters of MCDGRBM.

Step 1: Randomly initialize $\tilde{\mathbf{W}}$, $\tilde{\mathbf{b}}$ and $\tilde{\mathbf{c}}$.

Step 2: Sample the states of the hidden layer units by Eq. (31).

Step 3: Sample the states of the reconstructed visible layer units by Eq. (32).

Step 4: Update $\tilde{\mathbf{W}}$ parameter by Eq. (33).

Step 5: Update $\tilde{\mathbf{b}}$ parameter by Eq. (34).

Step 6: Update $\tilde{\mathbf{c}}$ parameter by Eq. (35).

Step 7: **While** iteration less than maximum **go to** Step 2.

step 8: **return** $\tilde{\mathbf{W}}$, $\tilde{\mathbf{b}}$ and $\tilde{\mathbf{c}}$.

4 DEEP SEMI-SUPERVISED FEATURE LEARNING WITH MINOR CONSTRAINT DISTURBANCES

In this section, we illustrate the novel deep semi-supervised feature learning framework, MCD-DSFL, which consists of a Gaussian linear visible layer and N binary hidden layers that is a stack of one MCDGRBM and $N - 1$ MCDRBMs without the use of fine-tuning strategy. Each of them has only one binary feature representation layer. The hidden layer features (\mathbf{h}_1) of the MCDGRBM are used as the input data for the next MCDRBM. Similarly, the hidden layer features ($\mathbf{h}_i, i = 2, 3, \dots, N - 1$) of the MCDRBM are used as the input data for the following MCDRBM. The architecture of the proposed MCD-DSFL is shown in Fig. 1. The reconstruction procedure of the MCDRBM adopts the sigmoid transform by 1 step Gibbs sampling. But we use a linear transform to reconstruct the visible layer of the MCD-DSFL framework. The hidden features of its deepest layer

(\mathbf{h}_N) is the input for the following learning task.

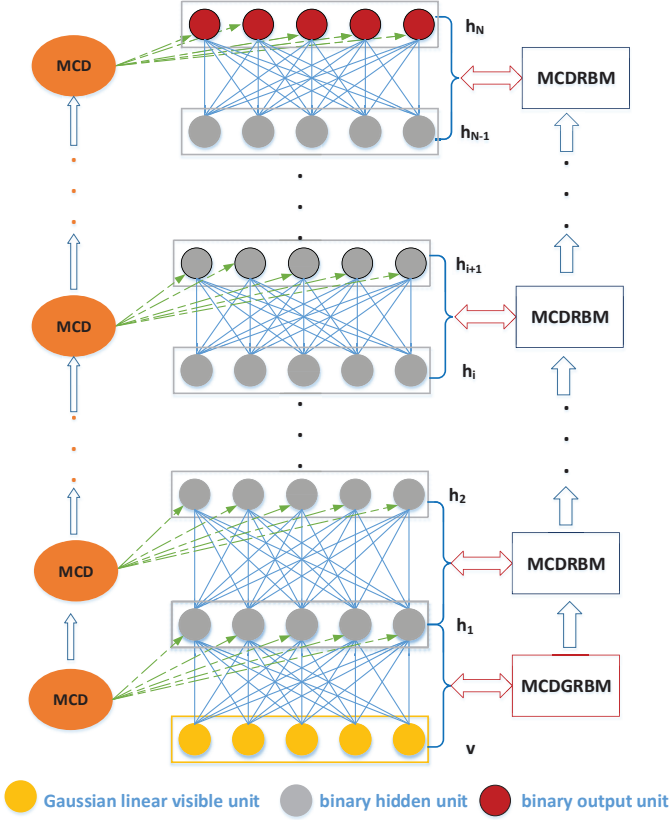


Fig. 1: The Minor Constraint Disturbances-based Deep Semi-supervised Feature Learning (MCD-DSFL) framework. It consists of a Gaussian linear visible layer and N binary hidden layers that is a stack of one MCDGRBM and $N - 1$ MCDRBMs. Each of them has only one binary feature representation layer which is the input data for the next MCDRBM.

5 EXPERIMENTS

To assess the performance of the proposed MCD-DSFL framework and compare it with state-of-the-art feature learning methods, we have conducted unsupervised and semi-supervised clustering experiments with fifteen image datasets (continuous data of global features) of the Microsoft Research Asia Multimedia image sub-dataset (MSRA-MM) [46]. They are listed in Table 1. For each data set, we only use less than 0.8% labels to generate the MCD for the MCD-DSFL framework. The labels usage ratios of them are in the range [0.6363%, 0.7126%].

We compare the MCD-DSFL framework with the benchmarking algorithms (e.g. spectral clustering (SP) [47], Semi-SP [48]), the shallow models (e.g. pcGRBM [19] and Semi-EAGR [49]) and the deep frameworks (e.g. DeepFS [15] and Semi-MG [34]). For all contrastive shallow models and deep frameworks, the performance evaluations have two stages: one is feature learning and the other is clustering analysis using SP algorithm. The output features of them are the input of SP algorithm.

Default depth of hidden layers of the MCD-DSFL framework is twenty-four ($N = 24$) in the experiments. The dimensionality of all hidden layers are the same as visible layer

TABLE 1: The summary of the fifteen image datasets

Dataset	Classes	Instance	Dimensions	Labels usage ratio
aquarium	3	922	892	0.6508%
banner	3	860	892	0.6977%
bathroom	3	924	892	0.6494%
bed	3	888	892	0.6757%
beret	3	876	892	0.6849%
blog	3	943	892	0.6363%
blood	3	866	892	0.6928%
boat	3	857	892	0.7001%
bonsai	3	867	892	0.6920%
bouquet	3	880	892	0.6818%
building	3	911	892	0.6586%
button	3	842	892	0.7126%
vegetable	3	872	899	0.6881%
voituretuning	3	879	899	0.6826%
wing	3	856	899	0.7009%

($m = n$). The learning rate ε is set to 10^{-3} . The scale coefficient γ varies from 0.12 to 0.96 with 0.12 per step ($\gamma \in (0.12, 0.24, 0.36, 0.48, 0.60, 0.72, 0.84, 0.96)$).

5.1 Evaluation Metrics

Four popular external evaluation metrics that are used in the paper to assess the experimental results are the clustering accuracy [50], Jaccard index (Jac index) [51], Fowlkes and Mallows index (FM index) [52] and recall [53]. Furthermore, the Friedman aligned ranks test [54]) is used to provide fair comparisons among different methods. The calculations of four external metrics are provided as follows:

- 1) The clustering accuracy metric is used to calculate the ratio of the instance assigned to the correct clusters. It is defined to be

$$accuracy = \frac{\sum_{i=1}^N F(l_i, l'_i)}{N}, \quad (36)$$

where N is the number of instances, l_i and l'_i are the target and predicted label, respectively, of the i th instance. If $l_i = l'_i$, then $F(l_i, l'_i) = 1$. Otherwise, $F(l_i, l'_i) = 0$.

- 2) The Jaccard Index measures similarity between sample sets can be written as

$$Jac = \frac{|A \cap B|}{|A \cup B|}, \quad (37)$$

where A and B are finite sample sets.

- 3) The Fowlkes and Mallows index calculates the similarity between the benchmark classifications and the clusters returned by the clustering algorithm. It is defined as

$$FMI = \sqrt{\frac{TP}{TP + FP} \times \frac{TP}{TP + FN}}, \quad (38)$$

where TP , FP and FN are the numbers of true positives, false positives and false negatives, respectively.

- 4) The recall metric is defined as the ratio of correctly assigned instances to the total number of relevant instances in the class. It is defined to be

$$Recall(i, j) = \frac{n_{i,j}}{n_i}, \quad (39)$$

where n_i is the total number of instances in class i , and $n_{i,j}$ is the number of correctly assigned instances of class i in cluster j .

The Friedman aligned ranks test is an advanced and popular nonparametric test method which can be used to analyze the performance of algorithms. It can be written as

$$T = \frac{(n-1)(\sum_{j=1}^n \hat{r}_j^2 - nn_a^2(nm+1)^2/4)}{nm(nm+1)(2nm+1)/6 - \sum_{i=1}^m \hat{r}_i^2/n}, \quad (40)$$

where \hat{r}_j is the total ranks of the i th data set, \hat{r}_i is the total ranks of the j th algorithm, n is the number of algorithm and m is the number of data set. The test statistic T is compared for significance with a chi-square distribution for $n-1$ degrees of freedom.

5.2 Clustering Performance

We first compare the MCD-DSFL framework with SP and Semi-SP algorithms to evaluate that its distributions of output features are whether or not more reasonable than visible layer data. Then, we compare the MCD-DSFL framework with the pcGRBM [19] and Semi-EAGR [49] for clustering to evaluate that its capability of the deep semi-supervised feature representation is whether or not more powerful than shallow feature representation of the contrastive models. Moreover, we compare the MCD-DSFL framework with the DeepFS [15] and Semi-MG [34] to evaluate that its capability of the deep semi-supervised feature representation is whether or not more excellent than start-of-art contrastive deep frameworks.

Fig. 2 presents the clustering accuracy, Jac, FM and recall comparison of the above benchmarking algorithms, shallow models and deep frameworks for clustering on fifteen image data sets. On the whole, we can see that the MCD-DSFL framework shows fairly competitive performances in all evaluation metrics. In particular, it shows super-high performance on some data sets (e. g. banner, blood, bathroom and so on). Surprisingly, the MCD-DSFL framework shows super-high performance for the recall metric on all data sets.

All results of clustering accuracy are listed in Table 2. On the whole, the average clustering accuracies of SP, Semi-SP, pcGRBM, Semi-EAGR, DeepFS and Semi-MG are 0.3992, 0.4159, 0.4249, 0.5341, 0.4886, 0.4756, respectively. However, the clustering accuracy of the MCD-DSFL framework increases to 0.6854. To compare with the SP and Semi-SP algorithms, the MCD-DSFL framework improves the performance by 28.62% and 26.95%, respectively. These results well demonstrates that its output features have reasonable distributions than visible layer data for clustering. In contrast to the pcGRBM and Semi-EAGR models, the MCD-DSFL framework improves the performance by 26.05% and 15.13%, respectively. Thus, the results indicate that the deep feature representation capability of the MCD-DSFL framework is more powerful than shallow feature representation of the contrastive models. To compare with the DeepFS and Semi-MG frameworks, the MCD-DSFL improves the performance by 19.68% and 20.98%, respectively. Hence, we can conclude that it has more excellent capability of deep feature representation than contrastive deep frameworks.

As shown in Table 3, the average Jac of SP, Semi-SP, pcGRBM, Semi-EAGR, DeepFS and Semi-MG are 0.2691, 0.2836,

0.2911, 0.3256, 0.3541 and 0.3044, respectively. However, the MCD-DSFL framework raises the Jac metric to 0.5336 significantly. In contrast to the SP and Semi-SP algorithms, it improves the performance by 0.2654 and 0.2500, respectively. These results demonstrates again that the output features of the MCD-DSFL framework have reasonable distributions than visible layer data for clustering. To compare with pcGRBM and Semi-EAGR models, it improves the Jac by 0.2425 and 0.2080, respectively. Furthermore, in contrast to DeepFS and Semi-MG frameworks, the MCD-DSFL improves the Jac by 0.1795 and 0.2292, respectively. Hence, these results illustrate that it has more outstanding deep semi-supervised feature representation capability than contrastive shallow models and deep frameworks.

In Table 4, the average FMs of SP, Semi-SP, pcGRBM, Semi-EAGR, DeepFS and Semi-MG are 0.4381 and 0.4515, 0.4610, 0.4981, 0.5252 and 0.4739, respectively. However, the average FM index of the MCD-DSFL framework is raised to 0.7184 significantly. In contrast to the SP and Semi-SP algorithms, it improves the performance by 0.2803 and 0.2669, respectively. To compare with the pcGRBM and Semi-EAGR models, it improves the FM by 0.2574 and 0.2203, respectively. Furthermore, in contrast to DeepFS and Semi-MG frameworks, the MCD-DSFL improves the FM by 0.1932 and 0.2445, respectively. Hence, these comparisons show that our MCD-DSFL has exciting deep semi-supervised feature representation capability.

The results of recall are presented in Table 5. The average recalls of SP, Semi-SP, pcGRBM, Semi-EAGR, DeepFS and Semi-MG are 0.3340, 0.3682, 0.3922, 0.5028, 0.4626 and 0.4409, respectively. However, the MCD-DSFL framework shows the super-high performance on all data sets. It raises the average recall to 0.9554 significantly. In contrast to the SP and Semi-SP algorithms, it improves the metric of average recall by 0.6214 and 0.5872, respectively. To compare with the pcGRBM and Semi-EAGR models, it improves the average recall by 0.5632 and 0.4526, respectively. Furthermore, in contrast to DeepFS and Semi-MG frameworks, the MCD-DSFL improves the metric of average recall by 0.4928 and 0.5145, respectively.

All experimental results have demonstrated that the MCD-DSFL is superior to benchmarking algorithms and the state-of-the-art shallow models as well as deep frameworks for clustering in terms of clustering accuracy, Jac, FM and recall.

5.3 The Friedman Aligned Ranks Test

In the experiments, the Friedman Aligned Ranks test is based on 15 datasets and 7 contrast algorithms of ranks. The average ranks provide a fair comparison of these algorithms. On average, the proposed MCD-DSFL ranks the first with the value of 8.2000; the Semi-EAGR, DeepFS and Semi-MG ranks the second, third and fourth, with the values of 28.2667, 44.0000 and 48.2667, respectively; and the fifth, sixth and the last are the pcGRBM, Semi-SP and SP with ranks 74.5333, 81.3333 and 86.4000, respectively. Under the null hypothesis, the Friedman Aligned Ranks test is used to check whether the metrical sum of aligned ranks are different from the average of total aligned rank $\bar{R}_j = 795$:

$$\begin{aligned} & \sum_{j=1}^k \hat{R}_{..j}^2 \\ &= 1296^2 + 1220^2 + 1118^2 + 660^2 + 424^2 + 724^2 + 123^2 \\ &= 5572621, \end{aligned} \quad (41)$$

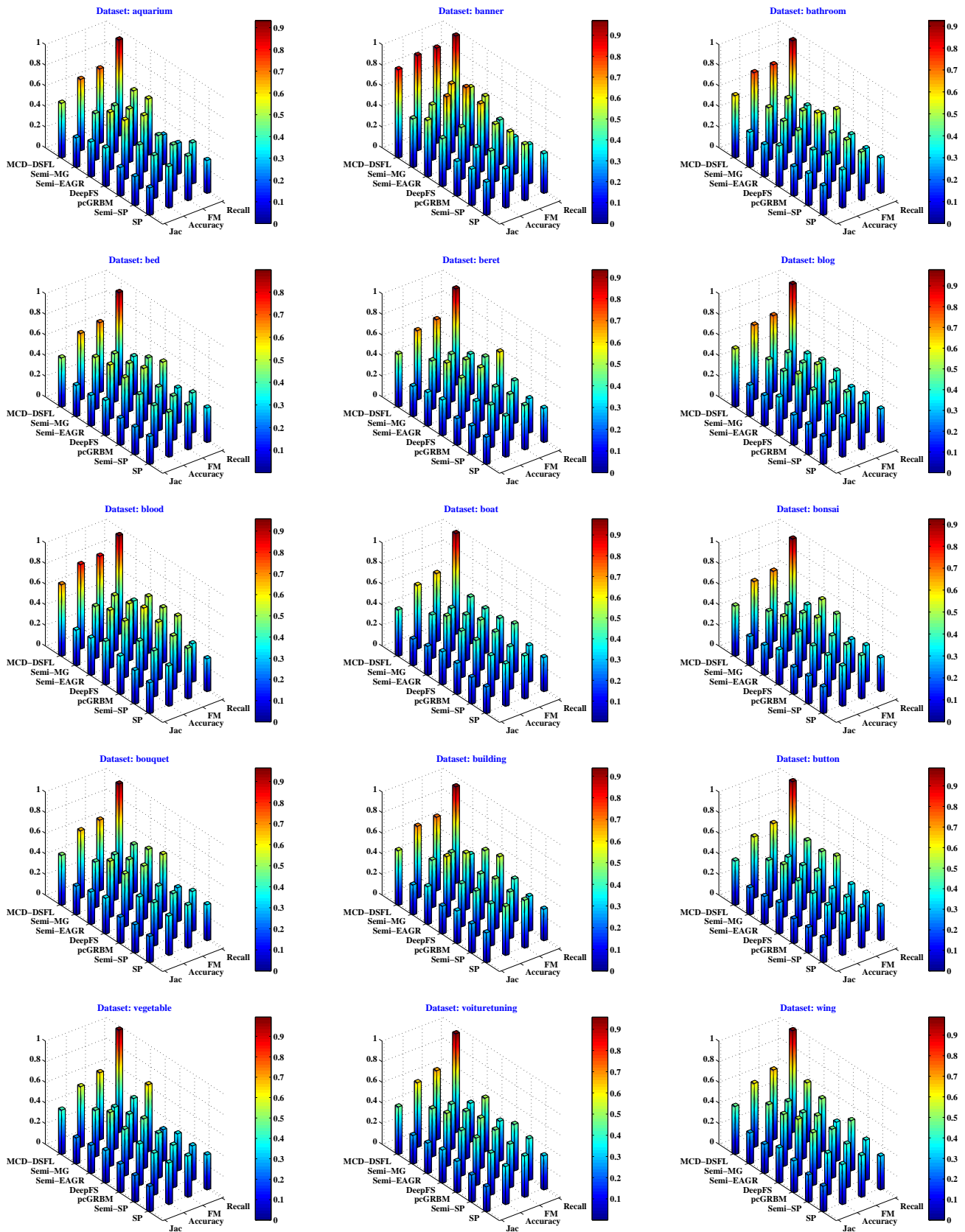


Fig. 2: Performance comparisons (Accuracy, Jac index, FM index and Recall) of benchmarking algorithms (SP and Semi-SP), shallow models (pcGRBM and Semi-EAGR), and deep frameworks (DeepFS, Semi-MG and our MCD-DSFL) on the MSRA-MM datasets. All external evaluation metrics are the mean values under different conditions of scale coefficient ($\gamma \in (0.12, 0.24, 0.36, 0.48, 0.60, 0.72, 0.84, 0.96)$).

TABLE 2: Performance comparisons (Accuracy) of benchmarking algorithms (SP and Semi-SP), shallow models (pcGRBM and Semi-EAGR), and deep frameworks (DeepFS, Semi-MG and our MCD-DSFL) on the MSRA-MM datasets. The larger clustering accuracy, the better performance. The best performance on each data set is bolded.

Dataset	SP [47]	Semi-SP [48]	pcGRBM [19]	DeepFS [15]	Semi-EAGR [49]	Semi-MG [34]	MCD-DSFL
aquarium	0.4028±0.0001	0.4169±0.0018	0.4287±0.0003	0.5738±0.0001	0.5561±0.0002	0.4544±0.0001	0.6925±0.0001
banner	0.3802±0.0002	0.4600±0.0056	0.4015±0.0067	0.5047±0.0001	0.7093±0.0006	0.5368±0.0002	0.9236±0.0001
bathroom	0.3701±0.0002	0.4333±0.0034	0.3780±0.0004	0.4751±0.0002	0.4722±0.0003	0.5110±0.0002	0.7576±0.0002
bed	0.4369±0.0001	0.4068±0.0012	0.4220±0.0002	0.4921±0.0001	0.5241±0.0001	0.5045±0.0001	0.6441±0.0001
beret	0.3972±0.0002	0.4132±0.0021	0.3556±0.0003	0.4886±0.0002	0.5431±0.0002	0.4717±0.0001	0.6716±0.0002
blog	0.3898±0.0001	0.4244±0.0031	0.4666±0.0002	0.5292±0.0001	0.4631±0.0009	0.4827±0.0001	0.7246±0.0001
blood	0.3912±0.0001	0.4462±0.0038	0.4469±0.0032	0.5485±0.0004	0.5603±0.0001	0.5050±0.0003	0.8193±0.0002
boat	0.4121±0.0001	0.3986±0.0009	0.4545±0.0004	0.4516±0.0002	0.5033±0.0001	0.4236±0.0002	0.6168±0.0001
bonsai	0.3900±0.0001	0.4012±0.0013	0.4008±0.0016	0.4441±0.0002	0.4993±0.0001	0.4581±0.0001	0.6548±0.0001
bouquet	0.3817±0.0001	0.4197±0.0015	0.3835±0.0013	0.5125±0.0001	0.5431±0.0002	0.4438±0.0002	0.6537±0.0001
building	0.4753±0.0005	0.4083±0.0023	0.4410±0.0078	0.4182±0.0003	0.5876±0.0001	0.4603±0.0002	0.6965±0.0003
button	0.3997±0.0001	0.3936±0.0010	0.4172±0.0048	0.4477±0.0002	0.5104±0.0002	0.4590±0.0002	0.5945±0.0002
vegetable	0.4037±0.0003	0.4058±0.0012	0.4034±0.0010	0.4518±0.0002	0.5222±0.0001	0.4511±0.0003	0.5875±0.0002
voituretuning	0.3691±0.0002	0.4059±0.0017	0.4613±0.0004	0.4403±0.0001	0.5135±0.0002	0.4657±0.0001	0.6259±0.0001
wing	0.3881±0.0002	0.4040±0.0015	0.5126±0.0038	0.5502±0.0002	0.5033±0.0001	0.5066±0.0001	0.6180±0.0001
Average	0.3992	0.4159	0.4249	0.4886	0.5341	0.4756	0.6854

TABLE 3: Performance comparisons (Jac index) of benchmarking algorithms (SP and Semi-SP), shallow models (pcGRBM and Semi-EAGR), and deep frameworks (DeepFS, Semi-MG and our MCD-DSFL) on the MSRA-MM datasets. The larger Jac, the better performance. The best performance on each data set is bolded.

Dataset	SP [47]	Semi-SP [48]	pcGRBM [19]	DeepFS [15]	Semi-EAGR [49]	Semi-MG [34]	MCD-DSFL
aquarium	0.2669	0.2827	0.2792	0.3767	0.3416	0.2891	0.5322
banner	0.3221	0.3556	0.3368	0.4671	0.5516	0.4732	0.8582
bathroom	0.2873	0.3132	0.2877	0.3967	0.3158	0.3428	0.6059
bed	0.2714	0.2691	0.2624	0.3449	0.2996	0.3033	0.4787
beret	0.2650	0.2809	0.2602	0.3496	0.3287	0.2948	0.5149
blog	0.2738	0.2956	0.2945	0.3773	0.2982	0.3050	0.5657
blood	0.3000	0.3264	0.3732	0.4237	0.3616	0.3459	0.6950
boat	0.2596	0.2589	0.3024	0.3224	0.2822	0.2590	0.4515
bonsai	0.2592	0.2713	0.2642	0.3420	0.2927	0.2844	0.4889
bouquet	0.2553	0.2758	0.2565	0.3491	0.3165	0.2792	0.4861
building	0.2908	0.2844	0.3170	0.2717	0.3680	0.2909	0.5322
button	0.2437	0.2498	0.2407	0.3063	0.2723	0.2637	0.4328
vegetable	0.2468	0.2585	0.2775	0.3173	0.2745	0.2546	0.4321
voituretuning	0.2448	0.2652	0.3044	0.3233	0.2963	0.2778	0.4625
wing	0.2495	0.2662	0.3102	0.3433	0.2843	0.3021	0.4677
Average	0.2691	0.2836	0.2911	0.3541	0.3256	0.3044	0.5336

TABLE 4: Performance comparisons (FM index) of benchmarking algorithms (SP and Semi-SP), shallow models (pcGRBM and Semi-EAGR), and deep frameworks (DeepFS, Semi-MG and our MCD-DSFL) on the MSRA-MM datasets. The larger FM, the better performance. The best performance on each data set is bolded.

Dataset	SP [47]	Semi-SP [48]	pcGRBM [19]	DeepFS [15]	Semi-EAGR [49]	Semi-MG [34]	MCD-DSFL
aquarium	0.4328	0.4489	0.4481	0.5477	0.5191	0.4582	0.7235
banner	0.5444	0.5734	0.5563	0.6628	0.7280	0.6679	0.9248
bathroom	0.4722	0.4958	0.4721	0.5736	0.5028	0.5283	0.7636
bed	0.4350	0.4287	0.4233	0.5129	0.4684	0.4692	0.6787
beret	0.4307	0.4458	0.4240	0.5184	0.5039	0.4634	0.7075
blog	0.4461	0.4666	0.4692	0.5492	0.4733	0.4796	0.7462
blood	0.4925	0.5176	0.5590	0.6043	0.5546	0.5388	0.8293
boat	0.4179	0.4143	0.4651	0.4879	0.4450	0.4160	0.6615
bonsai	0.4211	0.4336	0.4268	0.5098	0.4621	0.4508	0.6836
bouquet	0.4155	0.4370	0.4166	0.5176	0.4880	0.4433	0.6866
building	0.4651	0.4525	0.4863	0.4416	0.5491	0.4626	0.7143
button	0.3954	0.4013	0.3911	0.4700	0.4314	0.4188	0.6527
vegetable	0.3991	0.4118	0.4353	0.4829	0.4343	0.4086	0.6527
voituretuning	0.3994	0.4225	0.4672	0.4887	0.4624	0.4387	0.6719
wing	0.4049	0.4232	0.4746	0.5113	0.4487	0.4650	0.6791
Average	0.4381	0.4515	0.4610	0.5252	0.4981	0.4739	0.7184

TABLE 5: Performance comparisons (Recall) of benchmarking algorithms (SP and Semi-SP), shallow models (pcGRBM and Semi-EAGR), and deep frameworks (DeepFS, Semi-MG and our MCD-DSFL) on the MSRA-MM datasets. The larger recall, the better performance. The best performance on each data set is bolded.

Dataset	SP [47]	Semi-SP [48]	pcGRBM [19]	DeepFS [15]	Semi-EAGR [49]	Semi-MG [34]	MCD-DSFL
aquarium	0.3203	0.3985	0.2995	0.2880	0.5455	0.5332	0.9327
banner	0.3856	0.3797	0.3585	0.4340	0.5698	0.5629	0.9705
bathroom	0.3444	0.3421	0.3843	0.5370	0.4000	0.3858	0.9252
bed	0.3353	0.3895	0.3422	0.5027	0.4503	0.3699	0.8993
beret	0.3310	0.3327	0.4133	0.6010	0.4591	0.3924	0.9343
blog	0.3255	0.3778	0.3503	0.4172	0.4282	0.3967	0.9782
blood	0.3196	0.3723	0.5472	0.5360	0.5504	0.4160	0.9579
boat	0.3312	0.3527	0.4720	0.4333	0.4333	0.4544	0.9779
bonsai	0.3282	0.3539	0.3193	0.4737	0.5216	0.3772	0.9248
bouquet	0.3499	0.3869	0.3288	0.5600	0.5168	0.4680	0.9645
building	0.3061	0.3380	0.4128	0.5385	0.5051	0.3739	0.9378
button	0.3340	0.3687	0.3600	0.5438	0.4944	0.5073	0.9875
vegetable	0.3402	0.3349	0.3582	0.3060	0.6493	0.4229	0.9945
voituretuning	0.3312	0.4042	0.4500	0.3889	0.5190	0.3770	0.9580
wing	0.3273	0.3906	0.4872	0.3792	0.5140	0.5764	0.9885
Average	0.3340	0.3682	0.3922	0.4626	0.5038	0.4409	0.9554

TABLE 6: Performance comparisons (Rank) of benchmarking algorithms (SP and Semi-SP), shallow models (pcGRBM and Semi-EAGR), and deep frameworks (DeepFS, Semi-MG and our MCD-DSFL) on the MSRA-MM datasets. The smaller rank, the better performance.

Dataset	SP [47]	Semi-SP [48]	pcGRBM [19]	DeepFS [15]	Semi-EAGR [49]	Semi-MG [34]	MCD-DSFL	Total
aquarium	-0.1008 (97)	-0.0867 (90)	-0.0749 (84)	0.0701 (18)	0.0525 (23)	-0.0492 (64)	0.1889 (8)	384
banner	-0.1792 (105)	-0.0994 (95)	-0.1580 (104)	-0.0548 (68)	0.1499 (13)	-0.0226 (54)	0.3641(1)	440
bathroom	-0.1152 (101)	-0.0521 (65)	-0.1074 (98)	-0.0102 (47)	-0.0131 (50)	0.0257 (32)	0.2723(3)	396
bed	-0.0532 (66)	-0.0833 (87)	-0.0680 (81)	0.0021 (39)	0.0340 (29)	0.0144 (35)	0.1540 (11)	348
beret	-0.0801 (86)	-0.0641 (78)	-0.1217 (102)	0.0113 (36)	0.0658 (20)	-0.0056 (42)	0.1943 (6)	370
blog	-0.1074 (99)	-0.0728 (82)	-0.0306 (58)	0.0320 (30)	-0.0341 (60)	-0.0145 (52)	0.2274 (4)	385
blood	-0.1398 (103)	-0.0848 (89)	-0.0842 (88)	0.0174 (33)	0.0292 (31)	-0.0260 (56)	0.2882 (2)	402
boat	-0.0537 (67)	-0.0672 (80)	-0.0113 (48)	-0.0142 (51)	0.0375 (26)	-0.0422 (62)	0.1510 (12)	346
bonsai	-0.0741 (83)	-0.0629 (76)	-0.0632 (77)	-0.0200 (53)	0.0353 (28)	-0.0059 (43)	0.1907 (7)	367
bouquet	-0.0952 (94)	-0.0571 (71)	-0.0933 (92)	0.0356 (27)	0.0663 (19)	-0.0331 (59)	0.1769 (9)	371
building	-0.0229 (55)	-0.0899 (91)	-0.0572 (72)	-0.0800 (85)	0.0895 (17)	-0.0379 (61)	0.1983 (5)	386
button	-0.0606 (74)	-0.0667 (79)	-0.0431 (63)	-0.0126 (49)	0.0501 (24)	-0.0013 (40)	0.1342 (14)	343
vegetable	-0.0571 (70)	-0.0550 (69)	-0.0574 (73)	-0.0090 (45)	0.0615 (21)	-0.0097 (46)	0.1267 (15)	339
voituretuning	-0.0998 (96)	-0.0629 (75)	-0.0075 (44)	-0.0285 (57)	0.0447 (25)	-0.0031 (41)	0.1571(10)	348
wing	-0.1095(100)	-0.0935(93)	0.0150(34)	0.0527(22)	0.0057(38)	0.0091(37)	0.1204 (16)	340
Total	1296	1220	1118	660	424	724	123	5565
Average rank	86.4000	81.3333	74.5333	44.0000	28.2667	48.2667	8.2000	

$$\sum_{j=1}^k \hat{R}_{i..}^2 = 384^2 + 440^2 + 396^2 + 348^2 + 370^2 + 385^2 + 402^2 + 346^2 + 367^2 + 371^2 + 386^2 + 343^2 + 339^2 + 348^2 + 340^2 = 2076021, \quad (42)$$

$$T = \frac{(7-1)(5572621 - 7 \cdot 15^2(7 \cdot 15 + 1)^2/4)}{7 \cdot 15(7 \cdot 15 + 1)(2 \cdot 7 \cdot 15 + 1)/6 - 2076021/7} = 69.9273, \quad (43)$$

With seven algorithms and 15 data sets, T is a chi-square distribution with six degree-of-freedom. The null hypothesis is rejected because the p -value of T is 1.86×10^{-13} which is far less than 0.05. Therefore, we can conclude that these algorithms are significantly different.

5.4 Leverage Effect of the MCD

In Table 1, the labels usage ratios of all data sets are in the range [0.6363%, 0.7126%]. We use such less labels to generate the MCD which is applied to semi-supervised feature learning of the

MCDGRBM and MCDRBM models from the perspective of probability distribution. Fig. 3 presents the performance comparisons between visible and output layers of the MCD-DSFL framework on each data set. In visible layer of the proposed framework, the performance of average clustering accuracy, Jac, FM and recall are 0.3992, 0.2691, 0.4381 and 0.3340, respectively. However, these performances of output layer are significantly raised to 0.6854, 0.5336, 0.7184 and 0.9554, respectively. Despite the weak influence of the MCD for shallow MCDGRBM and MCDRBM models, all results show that the proposed MCD-DSFL framework improves the deep semi-supervised representation capability for clustering significantly. This means that the distributions of its output layer are more reasonable than visible layer. Most interestingly, the proposed framework shows high performances at low labels usage ratios. Results demonstrate that the MCD provide leverage in the training process of the MCD-DSFL framework. the MCD-DSFL framework indicates the leverage effect under the MCD for clustering.

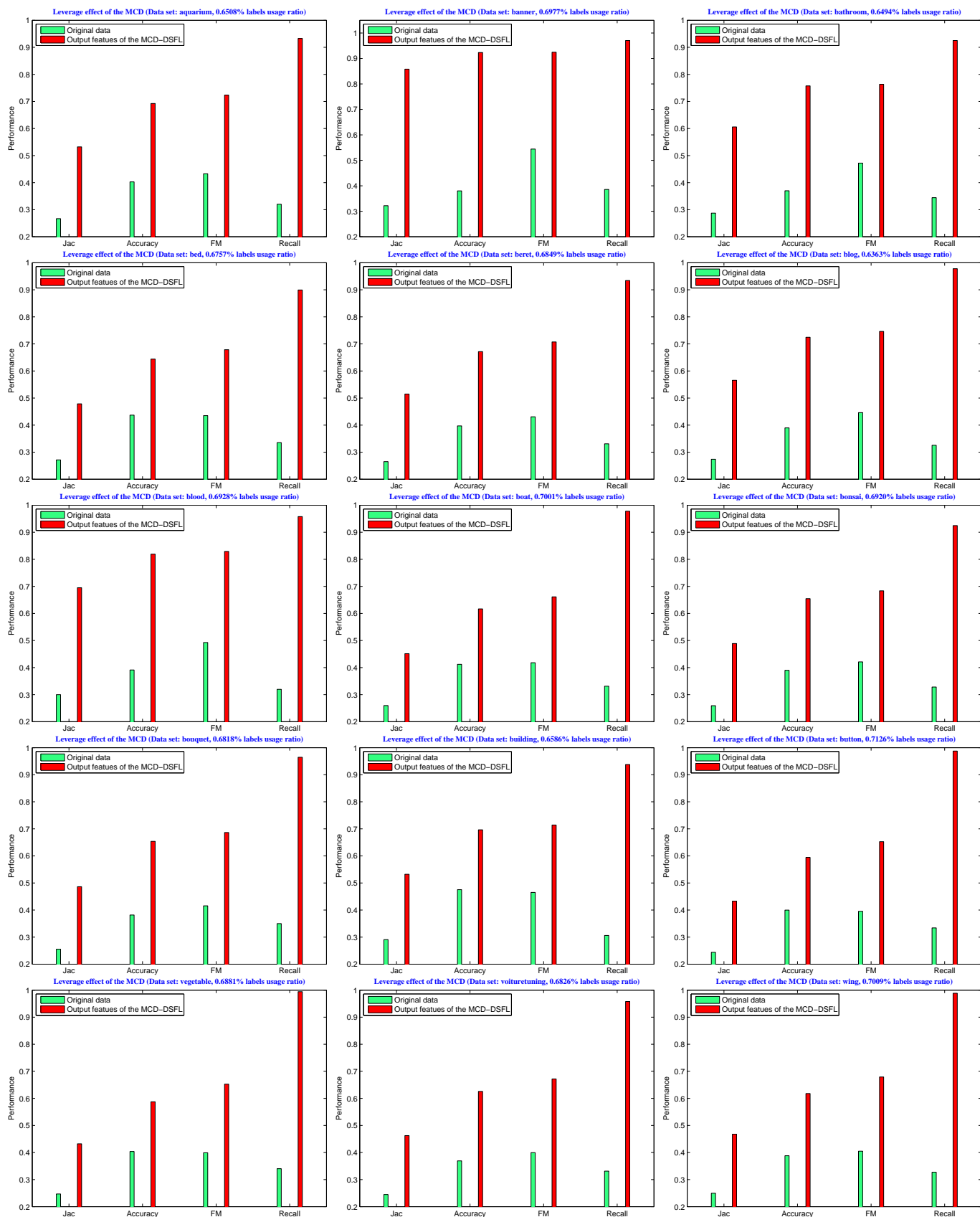


Fig. 3: Leverage effect of the MCD in the MCD-DSFL framework. High performances with low labels usage ratios ([0.6363%, 0.7126%]).

5.5 Sensibility of γ

To prove the sensibility and effectiveness of the scale coefficient γ , we gradually increase it from 0.12 to 0.96 with 0.12 per step in the learning process of the MCD-DSFL framework. We use SP algorithm to test the representation capability with the learned hidden features in the deepest layer. The performances of our framework are shown in Fig. 4. It is obvious that three external evaluation metrics (Accuracy, Jac and FM) steadily increase with γ . For external evaluation metric of recall, the general trend of the performance keeps increasing with γ except for $\gamma = 0.36$. On the whole, the scale coefficient γ shows positive effectiveness for the feature learning of the MCD-DSFL framework.

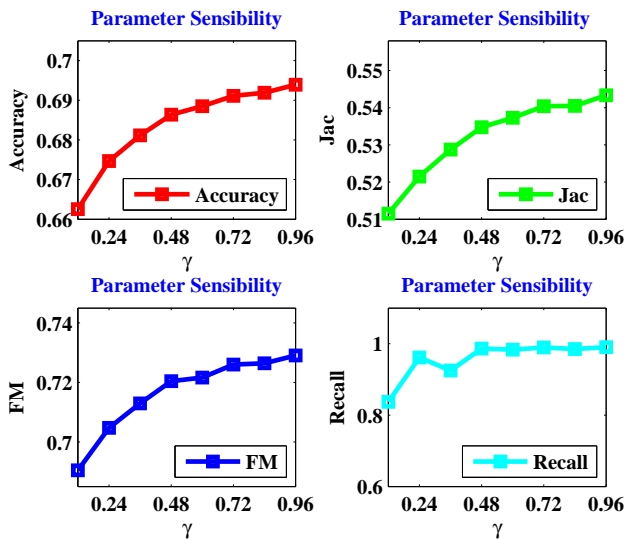


Fig. 4: The sensitivity of the scale coefficient (γ). It varies from 0.12 to 0.96 with 0.12 per step. The greater the γ , the greater the effect of the MCD on the MCD-DSFL framework.

6 CONCLUSIONS

We have presented MCD-DSFL, a deep semi-supervised feature learning framework from the perspective of probability distribution of the MCD using the fewest possible labels for modelling real-valued data. It consists of two fundamental modules: MCDGRBM and MCDRBM models. The MCD and CD learning are perfectly combined with each other in both of them. The semi-supervised feature representation capability of the MCD-DSFL framework is improved by the leverage effect of the MCD significantly. As a deep semi-supervised feature extractor, this framework can yield superior performances than the benchmarking algorithms for clustering. Furthermore, it shows more excellent capability of semi-supervised feature learning without the use of fine-tuning than other state-of-the-art shallow models and deep frameworks. Overall, the experimental results demonstrate the feasibility and effectiveness of this framework on fifteen image data sets.

In the future, there are several interesting works: 1) to explore adaptive learning strategy using internal evaluations to optimize feature distribution of hidden layer; 2) to study the theoretical support for which hidden layer of the deep framework has the best feature distribution; 3) to investigate fine-tuning strategy to further improve the performance of the proposed framework; 4) to extend the MCD-DSFL framework to model binary data.

7 ACKNOWLEDGEMENT

This work were partially supported by the National Science Foundation of China (Nos. 61773324, 61876158, 61806170) and Sichuan Science and Technology Program (2019YFS0432).

REFERENCES

- [1] C. Chen, Y. Gan, and C.-M. Vong, "Extreme semi-supervised learning for multiclass classification," *Neurocomputing*, vol. 376, pp. 103 – 118, 2020.
- [2] G. Giasemidis, N. Kaplis, I. Agrafiotis, and J. R. C. Nurse, "A semi-supervised approach to message stance classification," *IEEE Transactions on Knowledge and Data Engineering*, vol. 32, no. 1, pp. 1–11, Jan 2020.
- [3] F. Dornaika and L. Weng, "Sparse graphs with smoothness constraints: Application to dimensionality reduction and semi-supervised classification," *Pattern Recognition*, vol. 95, pp. 285 – 295, 2019.
- [4] C. Zhang, J. Cheng, and Q. Tian, "Unsupervised and semi-supervised image classification with weak semantic consistency," *IEEE Transactions on Multimedia*, vol. 21, no. 10, pp. 2482–2491, Oct 2019.
- [5] S. Liu, C. Ding, F. Jiang, Y. Wang, and B. Yin, "Auto-weighted multi-view learning for semi-supervised graph clustering," *Neurocomputing*, vol. 362, pp. 19 – 32, 2019.
- [6] Y. Ren, K. Hu, X. Dai, L. Pan, S. C. Hoi, and Z. Xu, "Semi-supervised deep embedded clustering," *Neurocomputing*, vol. 325, pp. 121 – 130, 2019.
- [7] S. Mittal, M. Tatarchenko, and T. Brox, "Semi-supervised semantic segmentation with high- and low-level consistency," *IEEE Transactions on Pattern Analysis and Machine Intelligence*, pp. 1–1, 2019.
- [8] J. Yang, S. Shebalov, and D. Klabjan, "Semi-supervised learning for discrete choice models," *IEEE Transactions on Intelligent Transportation Systems*, vol. 20, no. 11, pp. 4145–4159, Nov 2019.
- [9] S. Park, J. Lee, and K. Kim, "Semi-supervised distributed representations of documents for sentiment analysis," *Neural Networks*, vol. 119, pp. 139 – 150, 2019.
- [10] A. R. Kurup, M. Ajith, and M. M. Ramn, "Semi-supervised facial expression recognition using reduced spatial features and deep belief networks," *Neurocomputing*, vol. 367, pp. 188 – 197, 2019.
- [11] R. Razavi-Far, E. Hallaji, M. Farajzadeh-Zanjani, M. Saif, S. H. Kia, H. Henao, and G. Capolino, "Information fusion and semi-supervised deep learning scheme for diagnosing gear faults in induction machine systems," *IEEE Transactions on Industrial Electronics*, vol. 66, no. 8, pp. 6331–6342, Aug 2019.
- [12] F. Dornaika, K. Wang, I. Arganda-Carreras, A. Elorza, and A. Moujahid, "Toward graph-based semi-supervised face beauty prediction," *Expert Systems with Applications*, vol. 142, p. 112990, 10 2019.
- [13] R. Ito, K. Nakae, J. Hata, H. Okano, and S. Ishii, "Semi-supervised deep learning of brain tissue segmentation," *Neural Networks*, vol. 116, pp. 25 – 34, 2019.
- [14] Z. Zeng, X. Wang, F. Yan, and Y. Chen, "Local adaptive learning for semi-supervised feature selection with group sparsity," *Knowledge-Based Systems*, vol. 181, p. 104787, 2019.
- [15] A. Taherkhani, G. Cosma, and T. M. McGinnity, "Deep-fs: A feature selection algorithm for deep boltzmann machines," *Neurocomputing*, vol. 322, pp. 22–37, 2018.
- [16] L. Li and Z. Zhang, "Semi-supervised domain adaptation by covariance matching," *IEEE Transactions on Pattern Analysis and Machine Intelligence*, vol. 41, no. 11, pp. 2724–2739, Nov 2019.
- [17] Y. Jia, S. Kwong, J. Hou, and W. Wu, "Semi-supervised non-negative matrix factorization with dissimilarity and similarity regularization," *IEEE Transactions on Neural Networks and Learning Systems*, pp. 1–12, 2019.
- [18] X. Chen, G. Yuan, F. Nie, and Z. Ming, "Semi-supervised feature selection via sparse rescaled linear square regression," *IEEE Transactions on Knowledge and Data Engineering*, vol. 32, no. 1, pp. 165–176, Jan 2020.
- [19] J. Chu, H. Wang, H. Meng, P. Jin, and T. Li, "Restricted boltzmann machines with gaussian visible units guided by pairwise constraints," *IEEE Transactions on Cybernetics*, vol. 49, pp. 4321–4334, December 2019.
- [20] M. Jafar and K. Morteza, "Multiplicative distance: a method to alleviate distance instability for high-dimensional data," *Knowledge and Information Systems*, vol. 45, no. 3, pp. 783–805, 2015.

- [21] C. Huang, J. Chen, Y. Pan, H. Lai, J. Yin, and Q. Huang, "Clothing landmark detection using deep networks with prior of key point associations," *IEEE Transactions on Cybernetics*, vol. 49, no. 10, pp. 3744–3754, Oct 2019.
- [22] Y. Yuan, H. Ning, and X. Lu, "Bio-inspired representation learning for visual attention prediction," *IEEE Transactions on Cybernetics*, pp. 1–14, 2019.
- [23] M. Sun, Z. Zhou, Q. Hu, Z. Wang, and J. Jiang, "Sg-fcn: A motion and memory-based deep learning model for video saliency detection," *IEEE Transactions on Cybernetics*, vol. 49, no. 8, pp. 2900–2911, Aug 2019.
- [24] C. Low, J. Park, and A. B. Teoh, "Stacking-based deep neural network: Deep analytic network for pattern classification," *IEEE Transactions on Cybernetics*, pp. 1–14, 2019.
- [25] T. Ko and H. Kim, "Fault classification in high-dimensional complex processes using semi-supervised deep convolutional generative models," *IEEE Transactions on Industrial Informatics*, vol. 16, no. 4, pp. 2868–2877, April 2020.
- [26] X. Jia, X. Jing, X. Zhu, S. Chen, B. Du, Z. Cai, Z. He, and D. Yue, "Semi-supervised multi-view deep discriminant representation learning," *IEEE Transactions on Pattern Analysis and Machine Intelligence*, pp. 1–1, 2020.
- [27] Z. Chen, K. Wang, X. Wang, P. Peng, E. Izquierdo, and L. Lin, "Deep co-space: Sample mining across feature transformation for semi-supervised learning," *IEEE Transactions on Circuits and Systems for Video Technology*, vol. 28, no. 10, pp. 2667–2678, Oct 2018.
- [28] A. Sellami, M. Farah, I. R. Farah, and B. Solaiman, "Hyperspectral imagery classification based on semi-supervised 3-d deep neural network and adaptive band selection," *Expert Systems with Applications*, vol. 129, pp. 246 – 259, 2019.
- [29] B. Xue and N. Tong, "Diod: Fast and efficient weakly semi-supervised deep complex isar object detection," *IEEE Transactions on Cybernetics*, vol. 49, no. 11, pp. 3991–4003, Nov 2019.
- [30] H. D. Trinh, E. Zeydan, L. Giupponi, and P. Dini, "Detecting mobile traffic anomalies through physical control channel fingerprinting: A deep semi-supervised approach," *IEEE Access*, vol. 7, pp. 152 187–152 201, 2019.
- [31] Y. Meng, R. Shang, F. Shang, L. Jiao, S. Yang, and R. Stolkin, "Semi-supervised graph regularized deep nmf with bi-orthogonal constraints for data representation," *IEEE Transactions on Neural Networks and Learning Systems*, pp. 1–14, 2019.
- [32] G. Hinton and T. Sejnowski, "Learning and relearning in boltzmann machines," *Parallel distributed processing: Explorations in the microstructure of cognition*, vol. 1, pp. 282–317, 1986.
- [33] G. E. Hinton and R. R. Salakhutdinov, "Reducing the dimensionality of data with neural networks," *Science*, vol. 313, no. 5786, pp. 504–507, 2006.
- [34] P. Mercado, F. Tudisco, and M. Hein, "Generalized matrix means for semi-supervised learning with multilayer graphs," pp. 14 848–14 857, 2019.
- [35] P. Sankaran, S. Sunoj, and N. U. Nair, "Kullbackleibler divergence: A quantile approach," *Statistics and Probability Letters*, vol. 111, pp. 72 – 79, 2016.
- [36] M. Ponti, J. Kittler, M. Riva, T. de Campos, and C. Zor, "A decision cognizant kullbackleibler divergence," *Pattern Recognition*, vol. 61, pp. 470 – 478, 2017.
- [37] J. Collet, "An exact expression for the gap in the data processing inequality for f -divergences," *IEEE Transactions on Information Theory*, vol. 65, no. 7, pp. 4387–4391, July 2019.
- [38] P. Gurevich and H. Stuke, "Gradient conjugate priors and multi-layer neural networks," *Artificial Intelligence*, vol. 278, p. 103184, 2020.
- [39] K. K. Sharma and A. Seal, "Modeling uncertain data using monte carlo integration method for clustering," *Expert Systems with Applications*, vol. 137, pp. 100 – 116, 2019.
- [40] M. V. Giuffrida and S. A. Tsafaris, "Unsupervised rotation factorization in restricted boltzmann machines," *IEEE Transactions on Image Processing*, vol. 29, pp. 2166–2175, 2020.
- [41] A. Ahmadi and J. Tani, "A novel predictive-coding-inspired variational rnn model for online prediction and recognition," *Neural Computation*, vol. 31, no. 11, pp. 2025–2074, 2019.
- [42] G. E. Hinton, "Training products of experts by minimizing contrastive divergence," *Neural computation*, vol. 14, no. 8, pp. 1771–1800, 2002.
- [43] M. A. Carreira-Perpinan and G. E. Hinton, "On contrastive divergence learning," in *Proceedings of the Tenth International Workshop on Artificial Intelligence and Statistics*. Citeseer, 2005, pp. 33–40.
- [44] Y. Freund and D. Haussler, *Unsupervised learning of distributions of binary vectors using two layer networks*. Computer Research Laboratory [University of California, Santa Cruz], 1994.
- [45] J. Zhang, G. Tian, Y. Mu, and W. Fan, "Supervised deep learning with auxiliary networks," in *Proceedings of the 20th ACM SIGKDD international conference on Knowledge discovery and data mining*. ACM, 2014, pp. 353–361.
- [46] H. Li, M. Wang, and X.-S. Hua, "Msra-mm 2.0: A large-scale web multimedia dataset," in *Data Mining Workshops, 2009. ICDMW'09. IEEE International Conference on*. IEEE, 2009, pp. 164–169.
- [47] A. Y. Ng, M. I. Jordan, Y. Weiss *et al.*, "On spectral clustering: Analysis and an algorithm," *Advances in Neural Information Processing Systems*, vol. 2, pp. 849–856, 2002.
- [48] S. S. Rangapuram and M. Hein, "Constrained 1-spectral clustering," *arXiv preprint arXiv:1505.06485*, 2015.
- [49] M. Wang, W. Fu, S. Hao, D. Tao, and X. Wu, "Scalable semi-supervised learning by efficient anchor graph regularization," *IEEE Transactions on Knowledge and Data Engineering*, vol. 28, no. 7, pp. 1864–1877, July 2016.
- [50] Y. Lin, J. Jiang, and S. Lee, "A similarity measure for text classification and clustering," *IEEE Transactions on Knowledge and Data Engineering*, vol. 26, no. 7, pp. 1575–1590, July 2014.
- [51] F. O. de Franca, "A hash-based co-clustering algorithm for categorical data," *Expert Systems with Applications*, vol. 64, pp. 24 – 35, 2016.
- [52] R. Liu, H. Wang, and X. Yu, "Shared-nearest-neighbor-based clustering by fast search and find of density peaks," *Information Sciences*, vol. 450, pp. 200 – 226, 2018.
- [53] A. K. Abasi, A. T. Khader, M. A. Al-Betar, S. Naim, S. N. Makhadmeh, and Z. A. A. Alyasseri, "Link-based multi-verse optimizer for text documents clustering," *Applied Soft Computing*, vol. 87, p. 106002, 2020.
- [54] S. García, A. Fernández, J. Luengo, and F. Herrera, "Advanced non-parametric tests for multiple comparisons in the design of experiments in computational intelligence and data mining: Experimental analysis of power," *Information Sciences*, vol. 180, no. 10, pp. 2044–2064, 2010.



Jielei Chu received the B.S. degree from Southwest Jiaotong University, Chengdu, China in 2008, and is currently working toward the Ph.D. degree at Southwest Jiaotong University. His research interests include deep learning, semi-supervised learning and ensemble learning. He is a member of the IEEE.



Jing Liu received his Ph.D. degree in Management from Southwest Jiaotong University. She is currently an Assistant Professor of Business School in Sichuan University. Her research interests are machine learning, financial technology and modelling and forecasting high-frequency data.



Hongjun Wang received his Ph.D. degree in Computer Science from Sichuan University of China in 2009. He is currently an Associate Professor of the Key Lab of Cloud Computing and Intelligent Techniques in Southwest Jiaotong University. His research interests include machine learning, data mining and ensemble learning. He has published over 50 research papers in journals and conferences and he is a member of ACM and CCF.



Zhiguo Gong received the Ph.D. degree in Computer Science from the Institute of Mathematics, Chinese Academy of Science, Beijing, China. He is currently a Professor with the Faculty of Science and Technology, University of Macau, China. His current research interests include machine learning, data mining, database, and information retrieval.



Tianrui Li (SM'11) received the B.S., M.S., and Ph.D. degrees from Southwest Jiaotong University, Chengdu, China, in 1992, 1995, and 2002, respectively. He was a Post-Doctoral Researcher with Belgian Nuclear Research Centre, Mol, Belgium, from 2005 to 2006, and a Visiting Professor with Hasselt University, Hasselt, Belgium, in 2008; University of Technology, Sydney, Australia, in 2009; and University of Regina, Regina, Canada, in 2014. He is currently a Professor and the Director of the Key Laboratory

of Cloud Computing and Intelligent Techniques, Southwest Jiaotong University. He has authored or co-authored over 300 research papers in refereed journals and conferences. His research interests include big data, machine learning, data mining, granular computing, and rough sets.